Journal of ELECTRONIC MATERIALS, Vol. 46, No. 7, 2017
DOI: 10.1007/s11664-017-5466-0

Improvement of the Coercivity of Cobalt Ferrites Induced by Substitution of Sr^{2+} Ions for Co^{2+} Ions

KAIWEN ZHOU,[1,3] WEN CHEN,[1] XUEHANG WU,[2] WENWEI WU,[1,4,5] CUIWU LIN,[1] and JUAN WU[1]

1.—School of Chemistry and Chemical Engineering, Guangxi University, Nanning 530004, People's Republic of China. 2.—Collaborative Innovation Center of Renewable Energy Materials, Guangxi University, Nanning 530004, People's Republic of China. 3.—School of Materials Science and Engineering, Guangxi University, Nanning 530004, People's Republic of China. 4.—e-mail: gxuwuwenwei@aliyun.com. 5.—e-mail: wuwenwei@gxu.edu.cn

Spinel $Co_{1-x}Sr_xFe_2O_4$ (x = 0.0, 0.1, 0.2, and 0.3) ferrites have been successfully synthesized by calcining a mixture of oxalates in air. X-ray diffraction study shows that the sample with the concentration of x = 0 has a single spinel phase $CoFe_2O_4$ structure and the samples with concentrations of x = 0.1–0.3 have a small amount of foreign phase $SrFe_{12}O_{19}$ and/or $Sr_7Fe_{10}O_{22}$ along the spinel phase. The lattice parameter of the ferrites at first increases with increasing Sr^{2+} content, then decreases to x = 0.3 due to the large ionic radius of Sr^{2+} (0.144 nm) as compared to Co^{2+} (0.072 nm); for higher doping levels, part of the Sr^{2+} ions could not enter the tetrahedral (A) and/or octahedral (B) sites but forms a second phase $Sr_7Fe_{10}O_{22}$. The addition of Sr^{2+} ions decreases the average crystallite size of $Co_{1-x}Sr_xFe_2O_4$, which is attributed to the foreign phase $Sr_7Fe_{10}O_{22}$ and/or $SrFe_{12}O_{19}$ restraining the growth of the $Co_{1-x}Sr_xFe_2O_4$ crystallite. The trend of specific saturation magnetization (Ms), remanence (Mr), and anisotropy constant (K_{eff}) decreases with the increase in Sr^{2+} content, whereas that of coercivity is increased. In this study, $Co_{0.8}Sr_{0.2}Fe_2O_4$ obtained at 800°C exhibits the highest coercivity (1699.25 ± 40.78 Oe), and $Co_{0.7}Sr_{0.3}Fe_2O_4$ obtained at 900°C exhibits the highest squareness (0.470 ± 0.008).

Key words: Magnetic materials, magnetic properties, chemical synthesis, x-ray diffraction

INTRODUCTION

Spinel ferrites are one of the most important magnetic materials which have been widely used in many fields. For example, as magnetic drug carriers, information storage, magnetic separation, ferrofluids, electronic devices, microwave absorption materials, wastewater processing, sensors, medical diagnosis, and energy storage.[1-11] The structure of spinel ferrite is cubic closed-pack.[1] In spinel ferrites, 64 tetrahedral (A-site) and 32 octahedral interstitial sites (B-site) are occupied by oxygen ions. Out of this, 8 of tetrahedral (A-site) and 16 of octahedral (B-site) sites are occupied by the metal cations.[12] Spinel ferrites MFe_2O_4 can be expressed by the chemical formula $\left(M^{2+}_{1-\delta}Fe^{3+}_{\delta}\right)\left[M^{2+}_{\delta}Fe^{3+}_{2-\delta}\right]O^{2-}_4$,[1,12] where parentheses and square brackets indicate the cation sites of tetrahedral (A) and octahedral (B) coordination, respectively, and δ represents the degree of inversion defined as a fraction of the (A) sites occupied by Fe^{3+} ions.[1] The magnetic moment direction of spinel ferrite cations in the tetrahedral A-site is opposite to that in the octahedral B-site.[1,13] Therefore, the magnetic moment (η^N_B, μ_B) per unit formula can be estimated according to the following relationship: $\eta^N_B = M_B - M_A$, where M_B and M_A are the B and A sub-lattice magnetic moments (μ_B), respectively.[14,15] The magnetic properties of spinel

(Received September 5, 2016; accepted March 20, 2017; published online March 28, 2017)

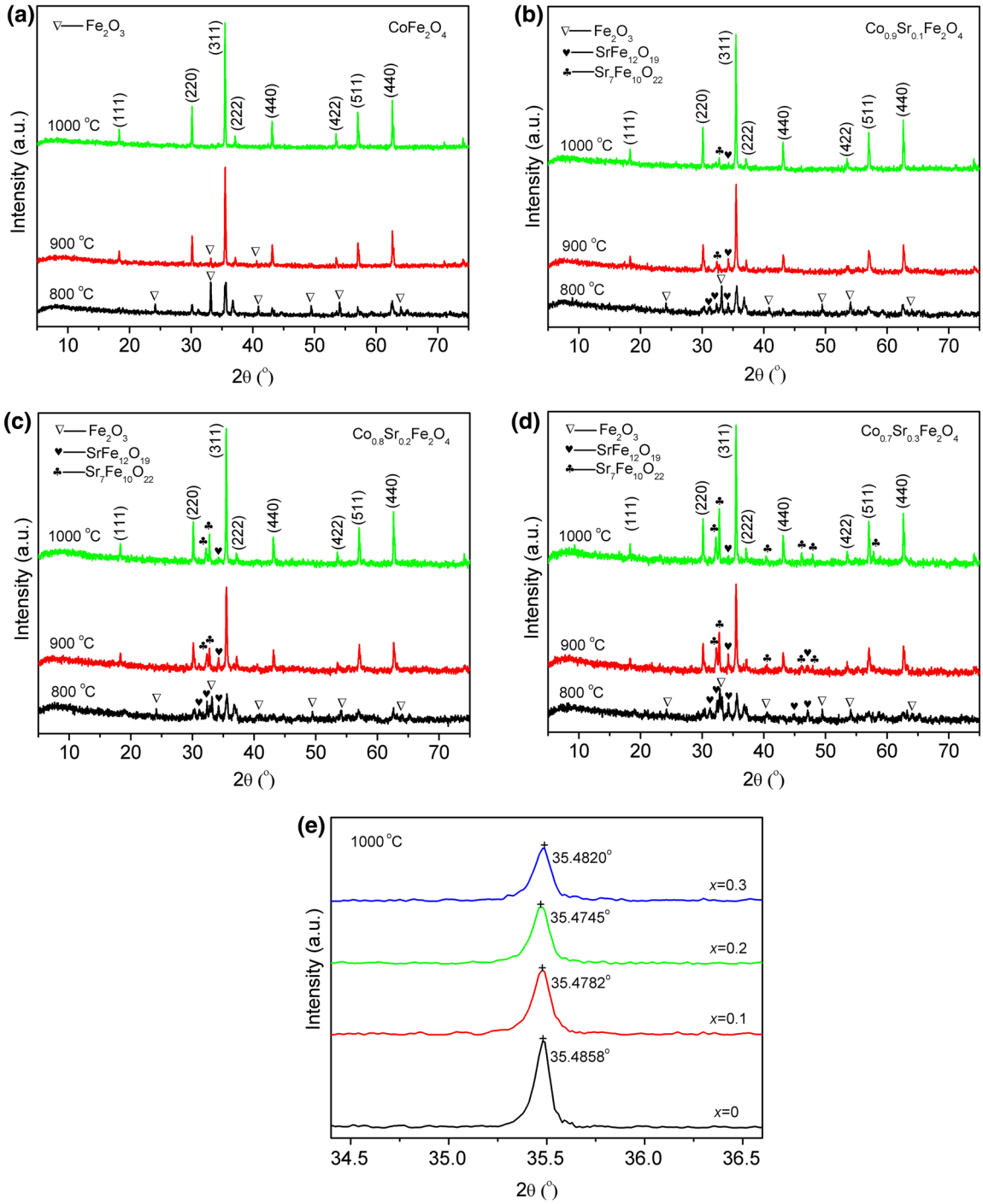

Fig. 1. (a)-(e) XRD patterns of $Co_{1-x}Sr_xFe_2O_4$: (a) $CoFe_2O_4$, (b) $Co_{0.9}Sr_{0.1}Fe_2O_4$, (c) $Co_{0.8}Sr_{0.2}Fe_2O_4$, (d) $Co_{0.7}Sr_{0.3}Fe_2O_4$, and (e) local magnification.

ferrites depend on various factors, for example, the synthesis method, chemical compositions, calcination temperature, and distribution of cations among the tetrahedral (A) and octahedral (B) sites. Among spinel ferrites, cobalt ferrite ($CoFe_2O_4$) is a very important hard magnetic material, which has many advantages, for example, great thermal stability, moderate specific saturation magnetization and squareness (Mr/Ms), large magnetocrystalline anisotropy and coercivity, and high values for Curie temperature, mechanical hardness, electric resistivity, and permeability.[16] In recent years, cobalt ferrite has largely been studied in the search for improved properties, and it has been found that doping cobalt ferrite can improve its magnetic properties.[16]

Various methods of synthesizing cobalt ferrite and doped cobalt ferrite with different morphology and magnetic properties have been developed, including solvothermal synthesis,[2,3] solid-state reaction,[4] evaporation method,[5] oxalates precursor method,[6] citrate precursor method,[7] co-precipitation method,[17] glycol-thermal technique,[18] combustion method,[19,20] sol–gel synthesis,[12,21] and hydrothermal treatment.[22,23] The substitution of Fe^{3+} ions in $CoFe_2O_4$ with diamagnetic ions is particularly interesting. For example, Pandit et al.[4] synthesized $CoAl_xFe_{2-x}O_4$ using a standard solid-state reaction technique. The samples exhibited ferrimagnetic behavior at 300 K and the specific saturation magnetization decreased with increasing Al^{3+} content. Kumar and Kar[8] synthesized mixed spinel La^{3+}-substituted $CoFe_2O_4$ nanoparticles by a citrate method. Crystallite size, magnetocrystalline anisotropy, specific saturation magnetization (Ms) and coercivity (Hc) decreased with the increase in La^{3+} content. Yang et al.[24] synthesized $(1-x)BaFe_{12}O_{19}/xCoFe_2O_4$ nanocomposite powders by a one-step sol–gel method. The results showed that substitution of Ba^{2+} ions for Co^{2+} caused a decrease in the Ms from 75.39 emu/g to 70.09 emu/g and the remanence (Mr) increased from 21.82 emu/g to 32.33 emu/g as Co^{2+} ion concentration was reduced from $x = 1$ to $x = 0.4$. However, the synthesis and magnetic properties of spinel $Co_{1-x}Sr_xFe_2O_4$ ($0.0 \le x \le 0.3$), obtained by calcining a mixture of oxalates in air have rarely been reported in previous studies.

Based on our previous works,[6] in this work, we have synthesized Sr^{2+}-substituted cobalt ferrites with the composition $Co_{1-x}Sr_xFe_2O_4$ (x = 0, 0.1, 0.2, and 0.3) by calcining a mixture of oxalates in air. Structural and magnetic property changes have been investigated with Sr^{2+} content and calcination temperature.

EXPERIMENTAL

$CoC_2O_4{\cdot}2H_2O$, $SrC_2O_4{\cdot}2H_2O$, and $FeC_2O_4{\cdot}2H_2O$ were used to synthesize $Co_{1-x}Sr_xFe_2O_4$ ferrites. All chemicals used were of reagent-grade purity (>99.9%). In a typical synthesis ($CoFe_2O_4$), 3.90 g $CoC_2O_4{\cdot}2H_2O$, 7.67 g $FeC_2O_4{\cdot}2H_2O$, and 5 mL ethanol were added to a stainless steel ball-milling tank of 100 mL. The mass ratio of the sample to stainless steel balls was about 1/15. Samples were milled at room temperature for 30 min. The grinding velocity was about 350 circles/min. The $CoFe_2O_4$ precursor was obtained after drying the mixture at 80°C in air for 4 h. A similar synthesis procedure was used to synthesize other $Co_{1-x}Sr_xFe_2O_4$ (x = 0.1, 0.2, and 0.3) precursors. Finally, the $Co_{1-x}Sr_xFe_2O_4$ precursor was calcined above 900°C for 2 h at a heating rate of 2°C min^{-1} in air to produce spinel $Co_{1-x}Sr_xFe_2O_4$.

Powder x-ray diffraction (XRD) patterns were recorded using X'pert PRO diffractometer at 40 kV and 50 mA using Cu Kα (λ = 1.5406 Å) radiation source. XRD scans were conducted from 5° to 75° in 2θ, with a step size of 0.01°. The morphology and particle size of the as-prepared samples were determined by a S-3400 scanning electron microscope (SEM) with an accelerating voltage of 15.0 kV. Magnetic measurements were performed using a Lake Shore 7410 vibrating sample magnetometer at room temperature with a maximum magnetic field of 20 kOe.

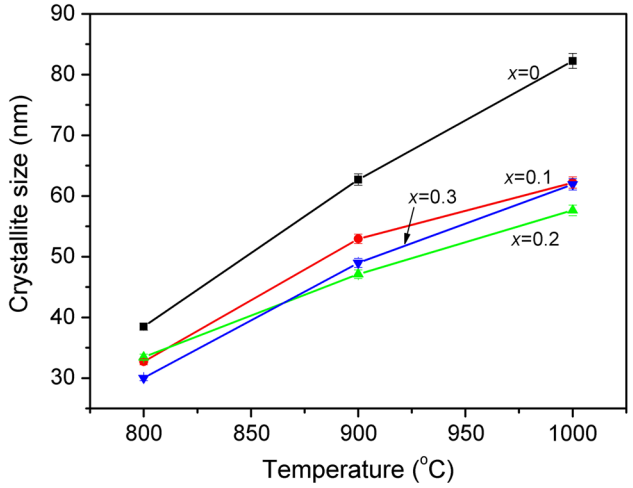

Fig. 2. Dependence of crystallite size of $Co_{1-x}Sr_xFe_2O_4$ on calcination temperature.

RESULTS AND DISCUSSION

XRD and SEM Analyses of the Calcined Products

Figure 1 shows the XRD patterns of calcined samples from different calcination temperatures for 2 h. XRD patterns in Fig. 1 show the existence of the (111), (220), (311), (222), (440), (422), and (511) and major crystal planes, which confirms the formation of the spinel cubic structure with the Fd3 m space group.[25] These patterns are compared with those of the standard (JCPDF) cards for Co ferrites. For $CoFe_2O_4$ (Fig. 1a), when the $CoFe_2O_4$ precursor was calcined at 1000°C, all diffraction peaks in the pattern were in accordance with those of cubic $CoFe_2O_4$ with space group Fd-3 m (227) from the JCPDF card 22-1086. Figure 2b–d shows the XRD patterns of $Co_{1-x}Sr_xFe_2O_4$ (x = 0.1, 0.2, and 0.3) from different calcination temperatures for 2 h, respectively. The results show that all the samples obtained at 1000°C consist of the main spinel phase in combination with a small amount of foreign $Sr_2Fe_{10}O_{22}$ and $SrFe_{11}O_{19}$ phases after doping with Sr^{2+} ions. This is because the ionic radius of Sr^{2+} ion (0.144 nm)[26] is much larger than that of the Co^{2+} ion (0.072 nm)[27] and the amount of Co^{2+} ions substituted by Sr^{2+} ions is limited, thus redundant Sr^{2+} ions aggregate on the grain boundaries forming $Sr_2Fe_{10}O_{22}$ and $SrFe_{12}O_{19}$ phases. The Sr^{2+}-doped ions do not change the spinel ferrite crystalline

Table I. Structural properties of $Co_{1-x}Sr_xFe_2O_4$ obtained at 1000°C

Composition	I_{220}/I_{222}	I_{422}/I_{222}	a (nm)	Lattice strains (%)
$CoFe_2O_4$	4.025(8)	1.324(3)	0.83918(3)	0.1377(6)
$Co_{0.9}Sr_{0.1}Fe_2O_4$	4.250(0)	1.203(1)	0.83918(9)	0.1636(7)
$Co_{0.8}Sr_{0.2}Fe_2O_4$	4.508(2)	1.311(5)	0.83919(6)	0.1637(2)
$Co_{0.7}Sr_{0.3}Fe_2O_4$	3.353(0)	0.882(4)	0.83919(1)	0.1650(3)

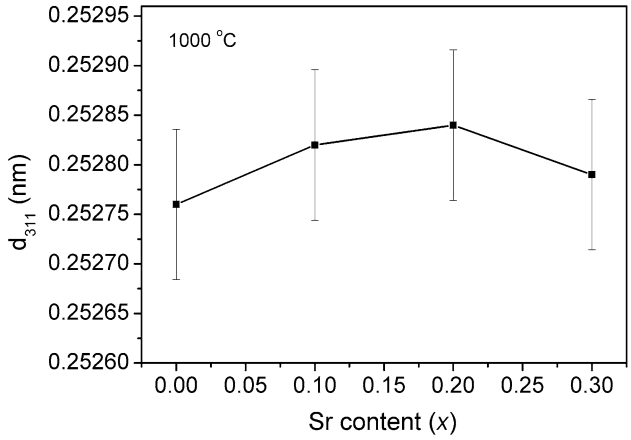

Fig. 3. Dependence of interplanar spacing (d_{311}) of $Co_{1-x}Sr_xFe_2O_4$ on Sr^{2+} content.

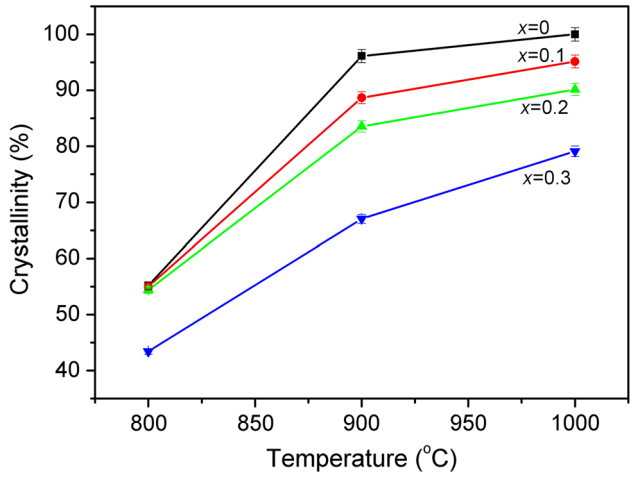

Fig. 4. Dependence of crystallinity of $Co_{1-x}Sr_xFe_2O_4$ on calcination temperature.

structure of MFe_2O_4 except that the diffraction peaks shift slightly to a lower degree with the increase of Sr^{2+} content between $x = 0$ and $x = 0.2$, then to higher degree at $x = 0.3$ (Fig. 1e). The lattice parameter of the sample was refined by the Rietveld analysis using MDI Jade (v.5.0) software.[1] The refined lattice parameter of $Co_{1-x}Sr_xFe_2O_4$, obtained at 1000°C, is listed in Table I. The lattice parameter increases with the increase in Sr^{2+} content except for $Co_{0.7}Sr_{0.3}Fe_2O_4$. The lattice parameter change of $Co_{1-x}Sr_xFe_2O_4$ can be explained on the basis of the ionic size difference of the component ions. The ionic radius of the Sr^{2+} ion (0.144 nm)[25] is much larger than that of the Co^{2+} ion (0.072 nm),[27] resulting in an increase of the $Co_{1-x}Sr_xFe_2O_4$ lattice parameter after doping with Sr^{2+} ions ($0 \le x \le 0.2$). However, the solubility limit of Sr^{2+} in the spinel lattice restrains that part of the Sr^{2+} ions filling the tetrahedral (A-site) and/or the octahedral sites (B-site), and redundant Sr^{2+} ions form the foreign phase $Sr_7Fe_{10}O_{22}$ and/or $SrFe_{12}O_{19}$, resulting in the decrease of the lattice parameter at a higher doping level ($x = 0.3$). A similar phenomenon was also observed for Sr^{2+}-doped Co-Ni spinel ferrites prepared by a reverse micelle process[28] and for Sr^{2+}-doped Zn ferrites prepared by a microwave combustion method.[29] The ratios of I_{220}/I_{222} and I_{422}/I_{222} are listed in Table I. The trend of I_{220}/I_{222} increases with the increase in Sr^{2+} content; and the ratio of I_{422}/I_{222} exhibits a nonlinear variation with Sr^{2+} content. This suggests that Sr^{2+} ions will prefer the occupation of the octahedral site.[1,30]

The crystallite size of $Co_{1-x}Sr_xFe_2O_4$ has been calculated according to the Scherrer formula[30,31]:

$$D = K\lambda/(\beta \cos\theta), \quad (1)$$

where D is the crystallite size, $K = 0.89$ (the Scherrer constant), $\lambda = 0.15406$ nm (wavelength of the x-ray used), β is the width of line at the half-maximum intensity, and θ is the corresponding angle.[1] The average crystallite size (D) of $Co_{1-x}Sr_xFe_2O_4$ is shown in Fig. 2. Average crystallite size of $Co_{1-x}Sr_xFe_2O_4$ increases with the increase of calcination temperatures. In addition, the average crystallite size of $Co_{1-x}Sr_xFe_2O_4$ decreases after doping with Sr^{2+}. This is because the foreign phase $Sr_7Fe_{10}O_{22}$ and/or $SrFe_{12}O_{19}$ increase with the increase in Sr^{2+} content, which restrains the growth of the $Co_{1-x}Sr_xFe_2O_4$ crystallite.

The $d_{(311)}$ interplanar spacing of $Co_{1-x}Sr_xFe_2O_4$ is determined using the following Bragg equation[32]:

$$d_{(311)} = \frac{\lambda}{2\sin\theta_{(311)}}, \quad (2)$$

The $d_{(311)}$ interplanar spacing of $Co_{1-x}Sr_xFe_2O_4$ increases with the increase in Sr^{2+} content between $x = 0$ and $x = 0.2$, and then, for a higher doping level at $x = 0.3$, $d_{(311)}$ interplanar spacing decreases (Fig. 3), which is attributed to the radius of Sr^{2+} ion (0.144 nm) being larger than that of the Co^{2+} ion

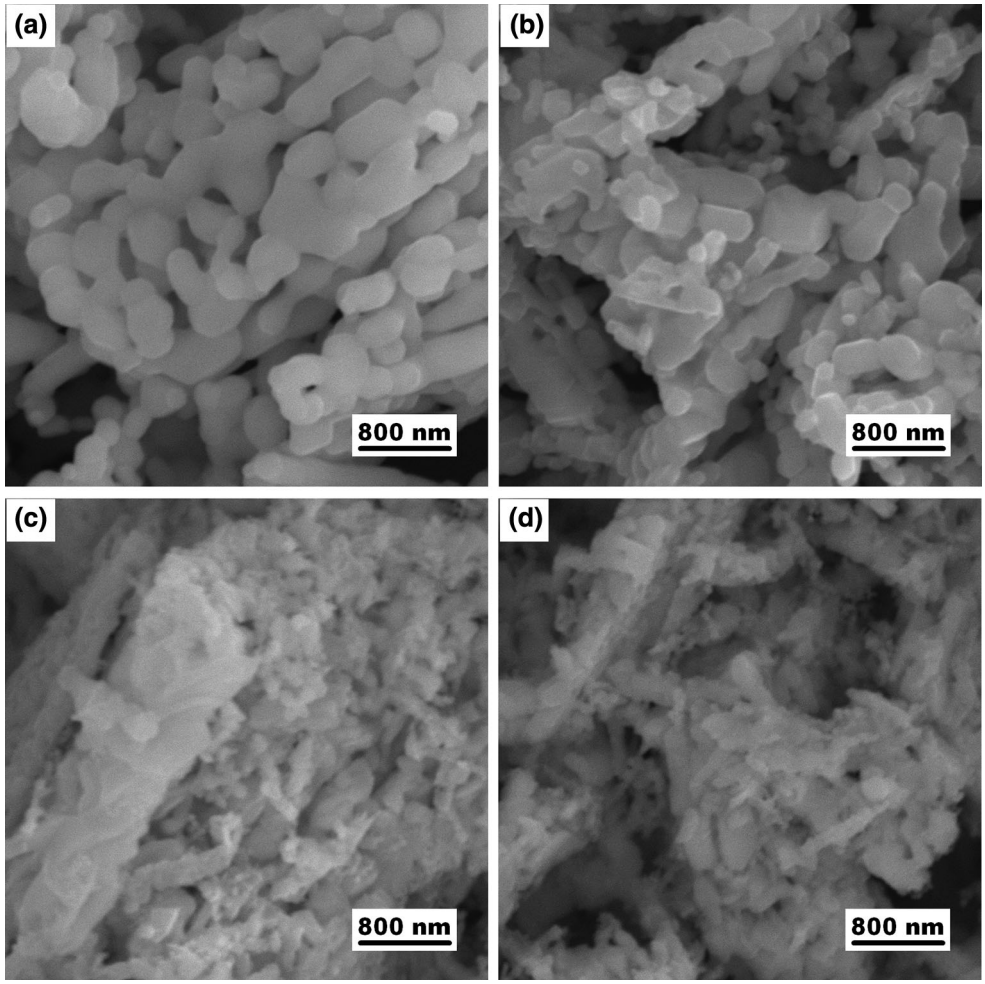

Fig. 5. SEM images of $Co_{1-x}Sr_xFe_2O_4$ obtained at 1000°C: (a) $CoFe_2O_4$, (b) $Co_{0.9}Sr_{0.1}Fe_2O_4$, (c) $Co_{0.8}Sr_{0.2}Fe_2O_4$, and (d) $Co_{0.7}Sr_{0.3}Fe_2O_4$.

(0.072 nm). The replacement of Co^{2+} ions in the tetrahedral A site and/or the octahedral (B) site by Sr^{2+} ions would cause the expansion of the unit cell, resulting in a larger $d_{(311)}$ value. However, with the increase in Sr^{2+} content ($x = 0.3$), part of the Sr^{2+} ions could not enter the tetrahedral (A) and/or the octahedral (B) sites but formed a second phase $Sr_7Fe_{10}O_{22}$, causing a lattice contraction and thus the decrease in the $d_{(311)}$ value.

The crystallinity of $Co_{1-x}Sr_xFe_2O_4$ has been estimated by MDI Jade (v.5.0) software according to the formula reported in the literature.[33,34] The crystallinity of $Co_{1-x}Sr_xFe_2O_4$ ($x = 0.0$, 0.1, 0.2, and 0.3) is shown in Fig. 4. The crystallinity of $Co_{1-x}Sr_xFe_2O_4$ increases with the increase in calcination temperature, and decreases with the increase in Sr^{2+} content. The crystallinities of $Co_{1-x}Sr_xFe_2O_4$ obtained at 1000°C are 100% for $x = 0.0$, 95.15 ± 1.14% for $x = 0.1$, 90.15 ± 1.08% for $x = 0.2$, and 79.11 ± 0.95% for $x = 0.3$, respectively.

Lattice strains of the $Co_{1-x}Sr_xFe_2O_4$ are estimated using the following Williamson–Hall formula[32]:

$$\varepsilon = \frac{\beta}{4\tan\theta}, \tag{3}$$

where β is the full width at half maximum (in radian) of the peaks, θ is the peak position, and ε is the lattice strain of the structure.[32] Lattice strains of $Co_{1-x}Sr_xFe_2O_4$ obtained at 1000°C are listed in Table I. The lattice strains of $Co_{1-x}Sr_xFe_2O_4$ increase with the increase in Sr^{2+} content, attributed to the radius of Sr^{2+} ion (0.144 nm) being much larger than that of the Co^{2+} ion (0.072 nm), resulting in the distortion of the tetrahedrons and octahedrons in $Co_{1-x}Sr_xFe_2O_4$ increasing with the increase in Sr^{2+} content.

Figure 5 shows the SEM images of $Co_{1-x}Sr_xFe_2O_4$ samples calcined at 1000°C for 2 h. It is shown that the particles of the samples with $x = 0$ and $x = 0.1$ bind together and display serious agglomeration without obvious particle boundaries. In addition, the particle sizes of the samples with $x = 0.2$ and $x = 0.3$ are between 100 nm and 200 nm, which are much smaller than that of the samples with $x = 0$ and $x = 0.1$, which indicates that the existence of

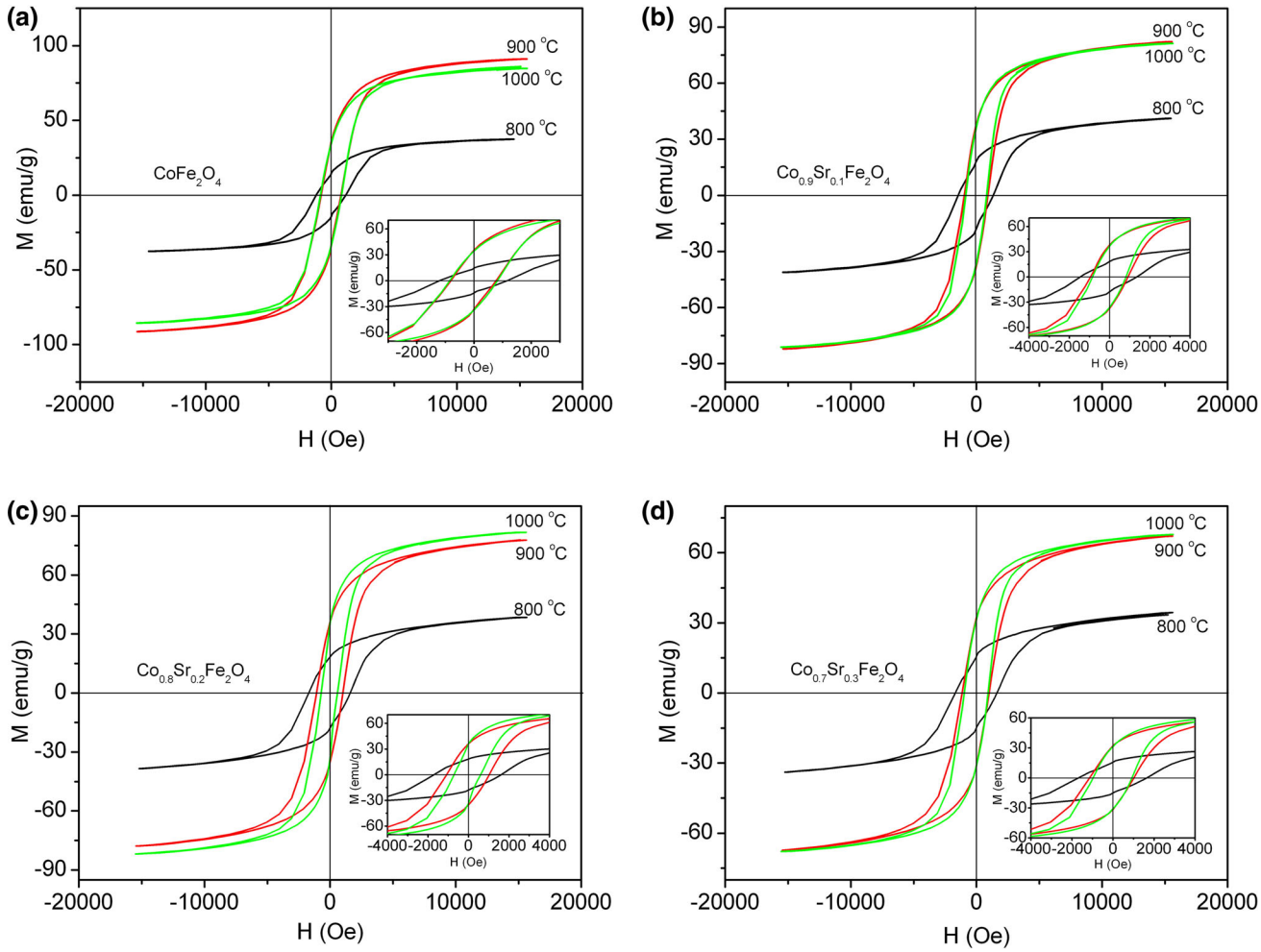

Fig. 6. *M-H* (magnetization-hysteresis) loops of $Co_{1-x}Sr_xFe_2O_4$ ($0.0 \le x \le 0.3$) samples obtained at different temperatures in air for 2 h: (a) $CoFe_2O_4$, (b) $Co_{0.9}Sr_{0.1}Fe_2O_4$, (c) $Co_{0.8}Sr_{0.2}Fe_2O_4$, and (d) $Co_{0.7}Sr_{0.3}Fe_2O_4$.

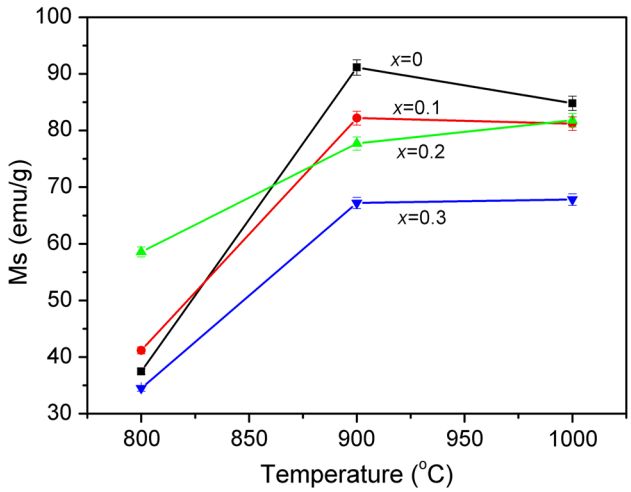

Fig. 7. Dependence of specific saturation magnetization of $Co_{1-x}Sr_xFe_2O_4$ on calcination temperature.

the foreign phase $Sr_7Fe_{10}O_{22}$ and/or $SrFe_{12}O_{19}$ restrains particle agglomeration.

Magnetic Properties of $Co_{1-x}Sr_xFe_2O_4$

Figure 6 shows the magnetization M (emu/g) of $Co_{1-x}Sr_xFe_2O_4$ as a function of the external magnetic field H (Oe). Magnetization of all the samples saturates below 10 kOe. Clear hysteric behavior and wide loops are observed, indicating the hard nature of these spinel ferrites. From these hysteresis loops, the specific saturation magnetization (Ms), coercivity (Hc), and remanence (Mr) can be obtained, and these values are shown in Figs. 7 and 8, respectively. Specific saturation magnetization of $CoFe_2O_4$ and $Co_{0.9}Sr_{0.1}Fe_2O_4$ increases with increasing calcination temperature between 800°C and 900°C, then, for a higher calcination temperature (1000°C), the specific saturation magnetization of $CoFe_2O_4$ and $Co_{0.9}Sr_{0.1}Fe_2O_4$ decreases slightly. In contrast, specific saturation magnetization of $Co_{0.8}Sr_{0.2}Fe_2O_4$ and $Co_{0.7}Sr_{0.3}Fe_2O_4$ increases with increasing

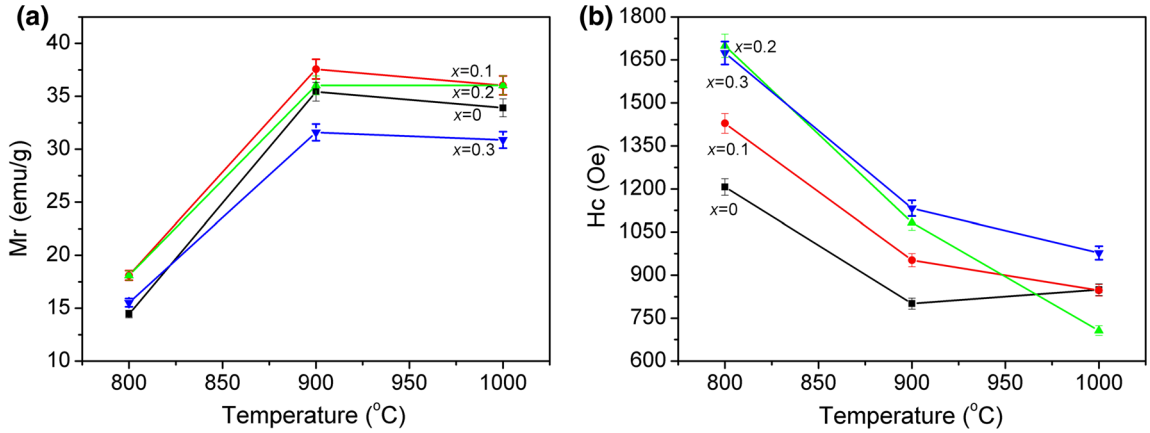

Fig. 8. Dependence of remanence (*Mr*) (a) and coercivity (*Hc*) (b) of $Co_{1-x}Sr_xFe_2O_4$ on calcination temperature.

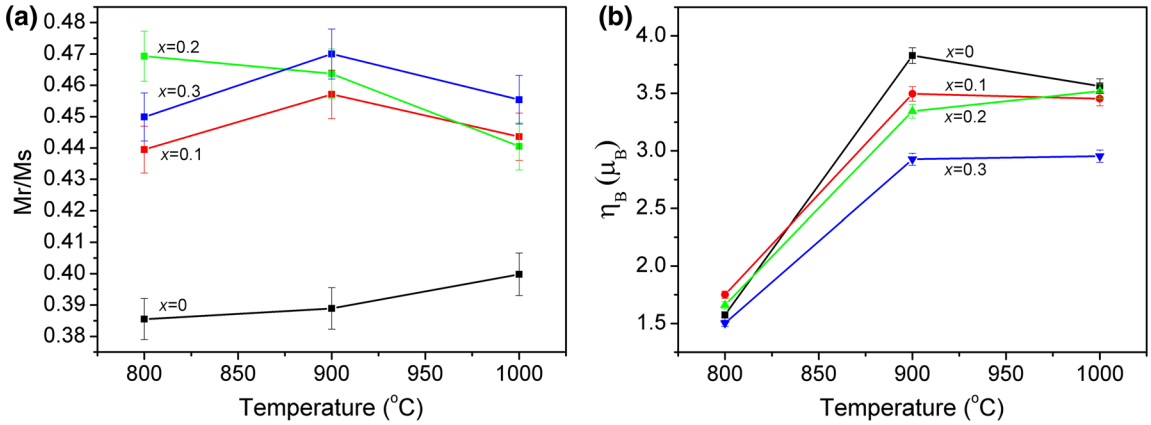

Fig. 9. Dependence of squareness (*Mr*/*Ms*) (a) and magnetic moment (η_B) (b) of $Co_{1-x}Sr_xFe_2O_4$ on Sr^{2+} content and calcination temperature.

calcination temperature. In addition, specific saturation magnetization of $Co_{1-x}Sr_xFe_2O_4$ decreases with increasing Sr^{2+} content (Fig. 7). Specific saturation magnetization changes of $Co_{1-x}Sr_xFe_2O_4$ with Sr^{2+} content can be explained as follows. First, weak magnetic $Sr_7Fe_{10}O_{22}$, lattice defects, and feeble magnetic superexchange interactions between A and B sites in the ferrites increase after doping with Sr^{2+} ions.[1] Second, substitution of Sr^{2+} ions with larger ionic radii for Co^{2+} ions on the B sites leads to lattice distortion and causes a reduction in the magnetic moment on the B sublattice.[35,36] Third, the disturbance exists in an antiferromagnetic exchange interaction of the ferrite lattice due to the substitution of ferromagnetic Co^{2+} ions on the B sites with diamagnetic Sr^{2+} ions. So, the net magnetic moment and/or specific saturation magnetization of spinel $Co_{1-x}Sr_xFe_2O_4$ decrease with increasing Sr^{2+} content.[1]

Remanence of $Co_{1-x}Sr_xFe_2O_4$ exhibits non-linearly variation (Fig. 8a). Remanence of $Co_{1-x}Sr_xFe_2O_4$ obtained at 900°C and 1000°C is between 30.88 ± 0.77 emu/g and 37.57 ± 0.94 emu/g. In contrast, the coercivity of $Co_{1-x}Sr_xFe_2O_4$ decreases with the increasing calcination temperature except for $CoFe_2O_4$ obtained at 1000°C, which increases after doping with Sr^{2+}. $Co_{0.8}Sr_{0.2}Fe_2O_4$, obtained at 800°C, has the highest coercivity value (1699.25 ± 40.78 Oe), while $Co_{0.8}Sr_{0.2}Fe_2O_4$ obtained at 1000°C has the lowest coercivity value (706.77 ± 16.96 Oe) (Fig. 8b). The value of coercivity increases after doping with Sr^{2+}, which is attributed to the decrease of crystallite size after doping with Sr^{2+} and coercivity is inversely proportional to the crystallite size.[36] In addition, the magnetic coercivity increases as the specific saturation magnetization decreases with Brown's relationship[12,37]:

$$Hc = \frac{2K}{\mu_0 Ms}, \tag{4}$$

where *Hc* is the coercivity, *K* is the anisotropy constant, *Ms* is the specific saturation magnetization, and μ_0 is the permeability.[1] The experimental results are consistent with Brown's relationship. In addition, foreign phase $Sr_7Fe_{10}O_{22}$ and/or $SrFe_{12}O_{19}$ is also an important factor affecting the coercivity of ferrite.[1] A similar phenomenon was also observed for Sr^{2+}-doped zinc ferrites[29] and Sr^{2+}-doped Mg-Mn

ferrites.[38] This is because impurities distributed in the grain boundary area break and go against the displacement of domain walls,[1] resulting in larger coercivity after doping with Sr^{2+} ions.

The dependence of squareness ($R = Mr/Ms$) on Sr^{2+} content is shown in Fig. 9a. After being calcined above 900°C, the trend of squareness (R) increases with the increase in Sr^{2+} content. $Co_{0.7}Sr_{0.3}Fe_2O_4$, obtained at 900°C, has the highest Mr/Ms (0.4700 ± 0.008). The R value reflects the magnetic domain type of ferrites. Larger R values ($R \geq 0.5$) indicate that ferrite is in a single magnetic domain. On the other hand, smaller R values ($R < 0.5$) are expected only in the case of the formation of a multi-domain structure.[38] The R values of all ferrites were below 0.5, which indicates that $Co_{1-x}Sr_xFe_2O_4$ (x = 0.0, 0.1, 0.2, and 0.3) particles are of a multi-domain type.[14,39]

The magnetic moment of $Co_{1-x}Sr_xFe_2O_4$ samples has been estimated using the following relationship [6,40]:

$$\eta_B = M \times Ms/5585, \quad (5)$$

where M is the molecular weight of the composition, and Ms is the specific saturation magnetization (emu/g), and η_B is the magnetic moment (μ_B).[1] The results are shown in Fig. 9b. The magnetic moment of $Co_{1-x}Sr_xFe_2O_4$ obtained at 900°C decreases with the increase in Sr^{2+} content. This is because the decrease of net magnetic moment of the octahedral (B) site after diamagnetic Sr^{2+} ion fills the octahedral B site and the increase of the weak magnetic $Sr_7Fe_{10}O_{22}$, lattice defects, and feeble magnetic superexchange interactions between the A and B sites in ferrites.[1,41] The magnetic moment of $Co_{1-x}Sr_xFe_2O_4$ obtained at 1000°C exhibits nonlinear variation. $CoFe_2O_4$ obtained at 900°C has the largest magnetic moment value (3.829 ± 0.069 μ_B).

The effective anisotropy constants (K_{eff}) were calculated using the following relationship[42]:

$$Hc = 0.985\frac{K_{eff}}{Ms}, \quad (6)$$

The anisotropy constant K_{eff} of $Co_{1-x}Sr_xFe_2O_4$ particles obtained at 1000°C is 73,154 ± 1756 erg/g for x = 0.0, 69,851 ± 1674 erg/g for x = 0.1, 58,687 ± 1408 for x = 0.2, and 67,290 ± 1615 for x = 0.3, respectively. The anisotropy constant K_{eff} decreases with the increase in Sr^{2+} content except for $Co_{0.7}Sr_{0.3}Fe_2O_4$. This is mainly because the specific saturation magnetization decreases with the increase of Sr^{2+} content.

CONCLUSIONS

Sr^{2+}-substituted cobalt ferrites particles $Co_{1-x}Sr_xFe_2O_4$ (x = 0.0, 0.1, 0.2, and 0.3) were synthesized by calcining a mixture of oxalates in air. X-ray powder diffraction examination confirms that a cubic spinel $Co_{1-x}Sr_xFe_2O_4$ is obtained when the precursor is calcined above 900°C in air for 2 h. The lattice parameter of the ferrites calcined at 1000°C slightly increases with increasing Sr^{2+} content, then decreases at x = 0.3. The change in lattice parameter at $x > 0.1$ indicates the solubility limit of Sr^{2+} in the spinel lattice, resulting in the formation of foreign phase $Sr_7Fe_{10}O_{22}$ and/or $SrFe_{12}O_{19}$. Specific saturation magnetization of $Co_{1-x}Sr_xFe_2O_4$ decreases with increasing Sr^{2+} content. This is because the weak magnetic $Sr_7Fe_{10}O_{22}$, lattice defects, and feeble magnetic superexchange interactions between the A and B sites in ferrites increase after doping with Sr^{2+} ions. However, coercivity (Hc) and squareness (M_r/M_s) are increased after doping with Sr^{2+} ions when the precursor is calcined at 800°C and 900°C. In this study, $Co_{0.8}Sr_{0.2}Fe_2O_4$ obtained at 800°C exhibits the highest coercivity (1699.25 ± 40.78 Oe) and $Co_{0.7}Sr_{0.3}Fe_2O_4$ obtained at 900°C exhibits the highest squareness (0.470 ± 0.008).

ACKNOWLEDGEMENTS

This study was financially supported by the National Natural Science Foundation of China (Grant Nos. 21603040, 21561003) and the Guangxi Natural Science Foundation of China (Grant Nos. 2016GXNSFDA380034, 2016GXNSFBA380062).

REFERENCES

1. W. Chen, W.W. Wu, D.S. Liu, and J. Wu, *J. Mater. Sci.: Mater. Electron.* 28, 2901 (2017).
2. N. Dong, F.Z. He, J.L. Xin, Q.Z. Wang, Z.Q. Lei, and B.T. Su, *Mater. Lett.* 141, 238 (2015).
3. L. Zhou, Q.Y. Fu, D.X. Zhou, F. Xue, and Y.H. Tian, *J. Magn. Magn. Mater.* 392, 22 (2015).
4. R. Pandit, K.K. Sharma, P. Kaur, R.K. Kotnala, J. Shah, and R. Kumar, *J. Phys. Chem. Solids* 75, 558 (2014).
5. E.R. Kumar, R. Jayaprakash, and R. Patel, *Superlattices Microstruct.* 62, 277 (2013).
6. W. Chen, Y. Zhou, J.Y. Lu, X.S. Huang, W.W. Wu, C.W. Lin, and Q. Wang, *Ceram. Int.* 42, 1114 (2016).
7. M.M. Rashad, R.M. Mohamed, and H. El-Shall, *J. Mater. Process. Technol.* 198, 139 (2008).
8. L. Kumar and M. Kar, *Ceram. Int.* 38, 4771 (2012).
9. X.H. Wu, W.W. Wu, Y.N. Li, F. Li, and S. Liao, *Mater. Lett.* 138, 192 (2015).
10. A.V. Malyshev, E.N. Lysenko, V.A. Vlasov, and S.A. Nikolaeva, *Ceram. Int.* 42, 16180 (2016).
11. S.F. Wang, Q. Li, X.T. Zu, X. Xiang, W. Liu, and S. Li, *J. Magn. Magn. Mater.* 419, 464 (2016).
12. R.S. Yadav, J. Havlica, J. Masilko, L. Kalina, J. Wasserbauer, M. Hajdúchová, V. Enev, I. Kuřitka, and Z. Kožáková, *J. Magn. Magn. Mater.* 399, 109 (2016).
13. W. Chen, W.W. Wu, S.Q. Liu, J.W. Xu, D.S. Liu, X.H. Wu, Y. Zhou, and J. Wu, *Mater. Sci. Semicond. Process.* 39, 544 (2015).
14. F. Saffari, P. Kameli, M. Rahimi, H. Ahmadvand, and H. Salamati, *Ceram. Int.* 41, 7352 (2015).
15. W. Chen, W.W. Wu, X.H. Wu, T.W. Li, J. Wu, and H.X. Zhang, *J. Mater. Sci.: Mater. Electron.* (2017). doi: 10.1007/s10854-017-6486-5.
16. W.W. Wu, J.C. Cai, X.H. Wu, S. Liao, and A.G. Huang, *Powder Technol.* 215–216, 200 (2012).
17. S. Chakrabarty, A. Dutta, and M. Pal, *J. Alloys Compd.* 625, 216 (2015).
18. N.S.E. Osman and T. Moyo, *Mater. Chem. Phys.* 164, 138 (2015).

19. Y. Zhang, Z. Yang, B.P. Zhu, W. Yu, S. Chen, X.F. Yang, and F. Jin, *Ceram. Int.* 40, 3439 (2014).
20. A.C. Lima, A.P.S. Peres, J.H. Araújo, M.A. Morales, S.N. Medeiros, J.M. Soares, D.M.A. Melo, and A.S. Carriço, *Mater. Lett.* 145, 56 (2015).
21. Z.L. Lu, P.Z. Gao, R.X. Ma, J. Xu, Z.H. Wang, and E.V. Rebrov, *J. Alloys Compd.* 665, 428 (2016).
22. E.C. Mendonça, Mayara A. Tenório, S.G. Mecena, B. Zucolotto, L.S. Silva, C.B.R. Jesus, C.T. Meneses, and J.G.S. Duque, *J. Magn. Magn. Mater.* 395, 345 (2015).
23. M. Penchal Reddy, A.M.A. Mohamed, X.B. Zhou, S. Du, and Q. Huang, *J. Magn. Magn. Mater.* 388, 40 (2015).
24. H.B. Yang, M. Liu, Y. Lin, and Y.Y. Yang, *J. Alloys Compd.* 631, 335 (2015).
25. H. Harzali, F. Saida, A. Marzouki, A. Megriche, F. Baillon, F. Espitalier, and A. Mgaidi, *J. Magn. Magn. Mater.* 419, 50 (2016).
26. B. Manoun, A. Ezzahi, S. Benmokhtar, A. Ider, P. Lazor, L. Bih, and J.M. Igartua, *J. Alloys Compd.* 533, 43 (2012).
27. X.S. Huang, Y. Zhou, W.W. Wu, J.W. Xu, S.Q. Liu, D.S. Liu, and J. Wu, *J. Electron. Mater.* 45, 3113 (2016).
28. A. Ghasemi, A. Paesano Jr, and C.F.C. Machado, *J. Magn. Magn. Mater.* 324, 2193 (2012).
29. A. Manikandan, J. Judith Vijaya, L. John Kennedy, and M. Bououdina, *Ceram. Int.* 39, 5909 (2013).
30. A.M. Wahba, N. Aboulfotoh Ali, and M.M. Eltabey, *Mater. Chem. Phys.* 146, 224 (2014).
31. X.S. Huang, W. Chen, W.W. Wu, Y. Zhou, J. Wu, Q. Wang, and Y.Y. Chen, *J. Mater. Sci.: Mater. Electron.* 27, 5395 (2016).
32. W. Chen, Y.Y. Chen, W.W. Wu, T.W. Li, C.Y. Zhang, Y. Zhou, and J. Wu, *J. Supercond. Nov. Magn.* 29, 115 (2016).
33. Y.L. Chai, Y.S. Chang, G.J. Chen, and Y.J. Hsiao, *Mater. Res. Bull.* 43, 1066 (2008).
34. X.Z. Guo, H. Yang, M. Cao, C. Han, and F.F. Song, *Trans. Nonferrous Met. Soc. China* 16, 593 (2006).
35. A.A. Kadam and K.Y. Rajpure, *J. Mater. Sci.: Mater. Electron.* 27, 10484 (2016).
36. R.C. Kambale, K.M. Song, Y.S. Koo, and N. Hur, *J. Appl. Phys.* 110, 053910 (2011).
37. M. Junaid, M.A. Khan, F. Iqbal, G. Murtaza, M.N. Akhtar, M. Ahmad, I. Shakir, and M.F. Warsi, *J. Magn. Magn. Mater.* 419, 338 (2016).
38. M.A. Amer, T.M. Meaz, S.S. Attalah, and A.I. Ghoneim, *J. Alloys Compd.* 654, 45 (2016).
39. T. Prabhakaran and J. Hemalatha, *Ceram. Int.* 40, 3315 (2014).
40. W. Chen, D.S. Liu, W.W. Wu, H.X. Zhang, and J. Wu, *J. Magn. Magn. Mater.* 422, 9 (2017).
41. A.A. Kadam, S.S. Shinde, S.P. Yadav, P.S. Patil, and K.Y. Rajpure, *J. Magn. Magn. Mater.* 329, 59 (2013).
42. X.H. Wu, W. Chen, W.W. Wu, H.J. Li, and C.W. Lin, *J. Electron. Mater.* 46, 199 (2017).